Acta Technica *62* (2017), No. 5A, 391–402

Research on night fatigue driving detection based on active infrared vision

Wang Guiping[2], Li Yuan[2], Wang Huifeng[2], Sun Weixuan[2]

Abstract. According to the low light and supplemental lighting of visible light which influence the natural driving, the fatigue driving detection based on active infrared vision is proposed. Firstly, in order not to affect the normal driving, the 940nm light source supply lighting, filter is selected to improve the quality of image and prevent interference of ambient light. Secondly, the existing fatigue detection algorithm is improved aiming at the acquired near-infrared image. Face location and tracing is realized with *ST_Adaboost* and *KLT* tracing algorithm. Then, eyes are located by gray-level integration method for *Gabor* transformation, which increases accuracy of eye location and tracking in active infrared image. Finally, the fatigue is judged by *PERCLOS* algorithm. The experiment results show that the proposed algorithm can detect fatigue driving around the clock, and the accuracy of eye positioning is more than 90%, the accuracy of eye status recognition is more than 87%. The proposed method can resolve the problem about driving fatigue at night, so there is great significance for the development of intelligent transportation and lowering the risk of traffic accidents especially at night.

Key words. Intelligent transportation, night driving fatigue, infrared active illumination, eye localization, klt tracking, gabor transform, parabolic fit.

1. Introduction

Fatigue driving has become the serious problem which causes accidents and threats human of their lives. According to statistics, 40% traffic accident was caused by fatigue driving, especially large and medium-sized truck and bus with more goods or passengers. They are the focus and difficulties of the traffic accident prevention due to the night driving produce fatigue easily. Therefore, the study of fatigue

[1]Acknowledgement - This work was supported by the Fundamental Research Funds for the Central Universities (No.310832162007), and Technology Project of Yunnan Transportation Department (No 2016(A)05).

[2]Workshop 1 - School of Electronic Control Engineering, Chang'an University, Xi'an, 710064, China

driving at night is significant.

As the light is weak and instability in the car, collected drivers' image signal-to-noise ratio is low with inconsistency data, while fatigue detection based on eye state recognition is very sensitive to the quality of images. In order not to affect recognition of object image, improve the image data consistency, combined with advantage of wavelet "digital microscope" and characteristics of fast template matching and strong parametric probability density with no parameters, a paper removed unknown noise in images that was taken at night. Some recognition systems taken the method of visible or near-infrared illumination[4], but brought new problems which the direction of illumination is strong and uniform resulting in poor *SNR*[5]. Hence, it is very limited to improve the image consistency.

The existing problems for fatigue early warning technology based on the eye states are long time consuming and less robust human eye tracking. *CSDS* detection method is proposed in a paper . It introduced verification and validation process and effectively control the occurrence of false reject under ensuring the detection rate, and improve the training speed. Zhang, Z. made use of nonlinear and traceless *Kalman* filter for eye tracking [6]. The improved algorithm can reduce the time of eye localization and improve the performance of eye tracking to some extent.

Aiming at the lack of research on the night fatigue warning and the application requirements, the following aspects of fatigue driving detection have been improved in this paper: analyze the infrared active light model, design a uniform supplement light system to solve poor image quality of face detection effectively at night, locate face with *Adaboost* algorithm, set the size threshold according to the experiments, reduce lots of unnecessary matching operations, and improve the speed of eye detection. The gray integral of *Gabor* transform locate eyes, weaken the effect of light changes on the test results, and improve the robustness of the system.

2. Active Infrared Uniform Illumination and Image Acquisition

2.1. The Infrared Uniform Illumination Field Model

Construct uniform illumination model by infrared *led* array. Firstly, determine a single infrared *led* illumination model. A single infrared *led* whose light-emitting size is small can be considered as a pointolite approximately relative to its lighting distance. The radiation distribution functionfor an ideal *led* pointolite is:

$$E\left(s,\theta\right)=E_0\left(\mathrm{s}\right)cos^m\theta \tag{1}$$

where $E\left(s,\theta\right)$ is the target radiation intensity of illumination s is the distance between the infrared LED and the target plane θ is the angle between the light and the optical axis $m{=}{-}ln2/ln(cos\theta_{1/2})$ is related to the $\theta_{1/2}$ the half decay angle $\theta_{1/2}$is the angle between the light and the optical axis when the radiation intensity is half of that in the $\theta{=}\,0$ direction, which is the intrinsic characteristics of the *led*. Generally, the value of m is greater than 1??$m \approx 1$??. When the infrared *led* irradiate

to a plane perpendicularly in the optical axis direction, the radiation distribution of *led* point light source can be converted into:

$$E(s,\theta) = \frac{I_{IRL} cos^m \theta}{h^2} \tag{2}$$

where h is the distance between the infrared *led* and the vertical plane of the target. I_{IRL} is the light intensity on *led* normal.

Take the center of infrared *led* array as origin to set up the Cartesian coordinate system, establish a tricyclic quaquaversal illumination model. The relationship between any *led* $(L_0(x_0, y_0, z_0))$ in *led* arrays and point $A(x, y, z)$in space is shown in fig. 1. R is the sphere for three-ring dome *led* array, α is the angle between L_0 normal and z axis (each ring has the same α), θ is L_0 after A point of light and L_0 optical axis Angle.

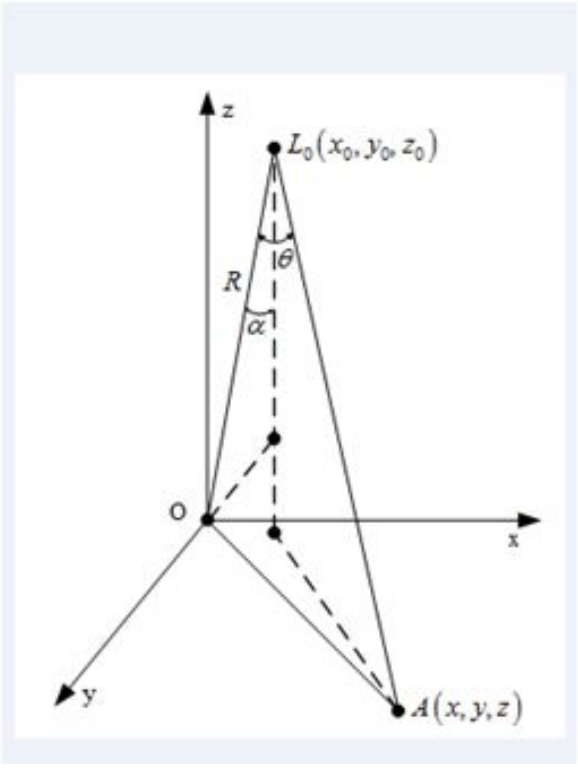

Fig. 1. The Geometrical Relationship of *ir-led* and point A

By the geometric relationships:

$$cos\theta = \frac{(x-x_0)^2 + (y-y_0)^2 + (Rcos\alpha - z)^2 + R^2 - \left(x^2 + y^2 + z^2\right)}{2R\left((x-x_0)^2 + (y-y_0)^2 + (Rcos\alpha - z)^2\right)^{1/2}} \tag{3}$$

$$h = \frac{(x-x_0)^2 + (y-y_0)^2 + (Rcos\alpha - z)^2 + R^2 - (x^2+y^2+z^2)}{2R} \tag{4}$$

Put (??)3) and (??)4) into (??)2) to calculate the illumination of point A within the L_0 radiation:

$$E(x,y,z) = I_{IRL} \frac{\left((x-x_0)^2 + (y-y_0)^2 + (Rcos\alpha - z)^2 + R^2 - (x^2+y^2+z^2)\right)^{m-2}}{\left((x-x_0)^2 + (y-y_0)^2 + (Rcos\alpha - z)^2\right)^{m/2} (2R)^{m-2}} \tag{5}$$

Due to the noncorrelation of infrared *led* light source, the light intensity of a point in the target area is the superposition of all infrared *led* light. The radiation distribution on the target surface can be expressed as

$$Q_t^n = 44.7x^{-0.150} \tag{6}$$

where N_i is the number of LEDs for each ring, α_i is located in the i ring of infrared leds normal line and z axis Angle. The radiation distribution of the whole area can be obtained by using the Eq. 6.

2.2. Uniform Lighting System Design

The image acquisition system based on infrared active illumination is shown in Fig. 2. It mainly includes: the infrared[7] *led* array light source, a diffusing panel, low illumination camera, band-pass filters and appropriate driving circuits.

As shown in Fig. 2(a), 1 is the diffusing panel (ring-like); 2 is 940 nm band-pass filter; 3 is the infrared *led* array (tricyclic quaquaversal) light source; 4 is the low illumination camera; 5 is the target area. Uniform diffusing panel and infrared led light source array compose the active illumination system, for lighting of the cab. The system also includes the 940 nm band-pass filter frame in front of the camera lens reducing the interference of ambient light, especially for street lighting and vehicle headlamps. It collects the images of driver in the infrared light. The whole system is an integrated structure, whose the driving circuit and the imaging subsystem are packaged in the *PVC* box, and the back has the standard *12V* power interface and video signal line output port. The material object as shown in Fig. 2(b).

The image acquisition device based on active infrared lighting has the following characteristics:

(1)Use the red 940 nm near-infrared lighting to drivers and unaffected their normal driving behavior. Moreover, the overlapping area between its spectrum and street light, sunlight and other vehicle lighting is small. Thus it's easy to shield other light.

(2)Multiple infrared *led* compose a tricyclic quaquaversal *led* arrays and embrace the camera in the middle. It will focus the light on the target in the center of the lighting area and expand the scope and intensity of lighting. Meanwhile, add the ring-like diffusing panel in the front of the *led* to improve uniformity of optical field

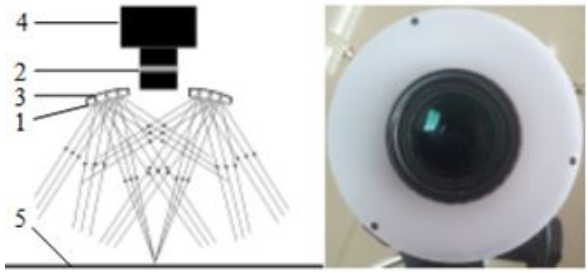

Fig. 2. The System Structure Diagram and its Actual Object

largely.

(3)Select 940nm band-pass filter. The center wavelength transmittance is above 90%. It can retain the active lighting into the camera while filter out different ambient light effectively.

2.3. Experimental Effect and Analysis of Uniform Illumination

The images of infrared active lighting experimental are shown in Fig. 3. The camera in the experiment is the *WATEC902H3* type low illumination camera with focal distance 3.6 and auto-iris lens. Fig. 3(a) was taken under natural light at night. Fig. 3(b) was acquired by ordinary infrared light source at night. Fig. 3(c) was acquired by tricyclic quaquaversal *led* arrays at night which added the diffuser in the front.

Fig. 3. The Imaging System and its effects

As can be seen from Fig.3, Fig. 3(a) is unavailable image relying on natural light at night whose noise is heavy. In Fig. 3(b), the ordinary active supplemental lighting improved the brightness and reduced the noise of the object region. However, the dazzle light occurred in the middle region which affect the processing and recognition of face region. In Fig. 3(c), we designed tricyclic quaquaversal *led* arrays based on the uniform illumination. Through the diffusing panel, the evenly light from all sides eliminate surface dazzle light effectively. So we can see the details of the human face clearly. Therefore, it is the foundation for the fatigue driving detection algorithm.

3. Eye Tracking and Positioning

3.1. Face Localization Based on ST_ Adaboost Algorithm

In the traditional *Adaboost* algorithm, when the training generated strong classifier locate or detect the face target, it is necessary to match and standardize the image at first, that is adjusting the size of the face in target image to complete the matching and location of the human eye. The system installation is shown in Fig. 4. In actual driving, the driver's space in the cab is limited. Accordingly, the distance between the driver's head and image collection system will change in a limited range, so the size of the image of target face detection in video fluctuate in a small range. As a result, we set the threshold value of the matching dimension of the human face image to reduce lots of unnecessary matching operations according to the experimental data. In this paper, the *Adaboost* algorithm which sets artificially matching size threshold of target image is called the *Size Threshold Adaboost* algorithm (*ST_ Adaboost*).

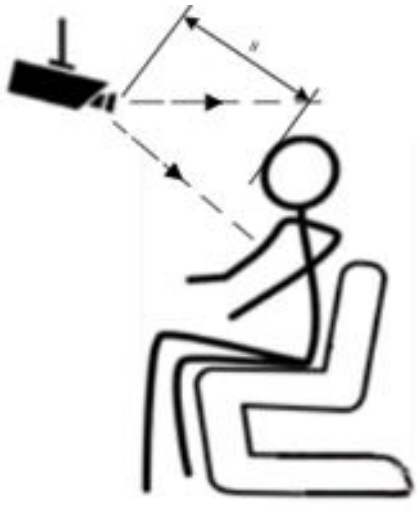

Fig. 4. The System Installation Sketch Map

By using the 10 test video (a total of 66 762 frames) in laboratory and cab, the paper carries on simulation experiments and compare the detection effect of the human eye pre and post threshold of matching size. The results are shown in Table 1.

Table 1. Test results contrast of the two algorithm

	Detection rate (%)	False reject rate (%)	Detection average time (ms)
Traditional Adaboost algorithm	91	5	48.5
ST_ Adaboost algorithm	95	3	332.3

The results showed that *ST_ Adaboost* algorithm of setting the threshold of matching size is superior to the traditional *Adaboost* algorithm, not only the correct rate of detection but the detection speed, which can improve system performance significantly.

3.2. KLT Face Tracking Algorithm Based on Harris Corner Point

In order to improve the speed of face localization, it tracks face window through the *KLT* track algorithm based on Harris corner after locating the face by *ST_ Adaboost* algorithm,

Harris operator detect the corner points by the differential operation and auto correlation matrix. It is simple calculation and gains the uniform and reasonable characteristics points, which is insensitive to image rotation, gray level change, noise effect and viewpoint transformation. The solving steps of the tracked face window based on Harris corner are as follows:

(1)Calculate the correlation matrix of each pixel in the face window M:

$$M = \begin{bmatrix} G(x,y)\ p_x^2 & G(x,y)\ p_x p_y \\ G(x,y)p_x p_y & G(x,y)\ p_y^2 \end{bmatrix} = \begin{bmatrix} A & C \\ D & B \end{bmatrix} \tag{7}$$

Where $\mathrm{G}(x,y) = \frac{1}{2\pi\sigma^2} e^{-(x^2+y^2)/2\sigma^2}$, P_x and P_y corresponds the pixel points respectively in the gradient of x, y direction

(2)Calculate the Harris corner response of each pixel in the face window

$$R = \frac{AB - CD}{A + B} \tag{8}$$

(3)Find the maximum value point in the face window. If the *Harris* corner point value is greater than the threshold value, it will be regarded as the corner point. A series of tracking point of *KLT* face tracking algorithms are obtained by solving the *Harris* corner points of the tracking face window.

Set face regional image at time t is $P(x,y)$, $t + \triangle t$ time face regional image is$Q(x,y)$. From t to $t + \triangle t$, the shift of characteristic $X(x,y)$ is $d = \triangle x, \triangle y$. Assuming that the face window in the image only takes place shifts and keeps the same brightness, the noise will be

$$n(X) = Q(X + d) - P(X) \tag{9}$$

What does the face window tracks is to solve the shift d to get the minimum $n(X)$.

Defined error value ε is:

$$\varepsilon = \int_W [n(X)]^2 = \int_W [Q(X+d) - P(X)]^2 \tag{10}$$

Where w is a feature window whose center is feature point $X(x, y)$.

Take Taylor expansion of $Q(X+d)$ into formula (10). When the differential of a is 0, bgets minimum, and we get the formula likec. Where

$$Z = \int_W \begin{bmatrix} {Q_x}^2 & Q_x Q_y \\ Q_x Q_y & {Q_y}^2 \end{bmatrix}, \; e = \int_W Q_l \begin{bmatrix} Q_x & Q_y \end{bmatrix}^T \tag{11}$$

Q_x, Q_y is the derivatives of $Q(x, y)$ in the direction of x and y respectively, Q_l is the difference between the 2 frame image pixels. While $d = Z^{-1}e$.

Assuming that in the video, $P$and Q are face regions in the two frame image pre and post, regard W as the little window by 3×3. Feature point $X(x, y)$ as tracking point, the 8 points around which were calculated. Luminance difference is

$$l_i \quad P_i \quad Q_i \quad i128 \tag{12}$$

The value of horizontal gradients plus vertical gradients is

$$g_{xi} \quad P_{xi} \quad Q_{xi} \quad g_{yi} \quad P_{yi} \quad Q_{yi} \quad i128 \tag{13}$$

Hence

$$z = \begin{bmatrix} \int_{i=1}^{8} g_{xi}{}^2 & \int_{i=1}^{8} g_{xi} g_{yi} \\ \int_{i=1}^{8} g_{xi} g_{yi} & \int_{i=1}^{8} g_{yi}{}^2 \end{bmatrix} = \begin{bmatrix} a & c \\ c & b \end{bmatrix},$$

$$e = \begin{bmatrix} \int_{i=1}^{8} l_i g_{xi} \\ \int_{i=1}^{8} l_i g_{yi} \end{bmatrix} = \begin{bmatrix} e_x \\ e_y \end{bmatrix} \tag{14}$$

The displacement is

$$d = Z^{-1}e = \frac{1}{abc^2} \begin{bmatrix} be_x & ce_y \\ ae_y & ce_x \end{bmatrix} = \begin{bmatrix} x \\ y \end{bmatrix} \tag{15}$$

Obtained the displacement of all tracking points, the face region of the two frame image can be determined. That is the tracking of the human face region in the image.

3.3. Eyes Location Based on Gray-Level Integration Combine with Gabor Transform

Human face area were located or tracked firstly, the feature of eyes by *Gabor* filtering was extracted and coarse localization is achieved. Combined with gray-level integration and edge detection eyes location is realized finally.

The location of left eye for example, the precisely location of the human eye is shown in Fig. 5. Fig. 5(a) is the face region after the *Gabor* transform. The image

mainly outstands eyebrows, eyes, nose and mouth. Then, it has simple filtration, gray scaling, erosion and dilation and results in Fig. 5(b). The position of eyes, nose and mouth is determined. According to the structure of the human face, we can locate the human eye area which is the horizontal integral projected to find the coordinates of the center of the pupil. All of the inherent characteristics of the human eye, the size of the image and the angle of the camera can get the upper and lower limits of the human eye while E_u=Y_m−6, E_d=Y_m+8. *Canny* edge detection on facial region between E_u ~ E_d then vertical integration projections for the result. Accurate positioning of the human eye is shown in Fig. 5(c)

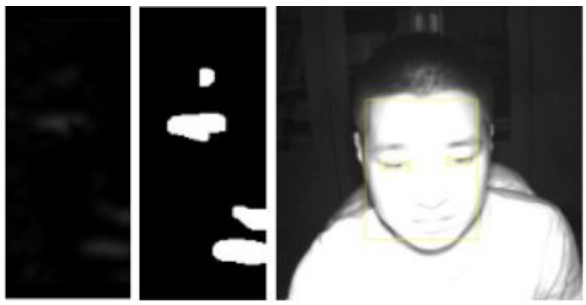

Fig. 5. The Accurate Positioning of eye

4. Feature Extraction and Determination of Fatigue

4.1. Feature Extraction of Fatigue

After located eye region precisely, the pixel points of the region in original image is too few, which is difficult to extract fatigue feature. Amplify the human eye area 25 times, eyes-open is shown in Fig. 6(a) and eyes-close is shown in Fig. 6(b). *Canny* edge detection on amplified eye area. Contour detection result on eyes-open is shown in Fig. 6(c). The upper and lower eyelids can be seen clearly. Contour detection result on eyes-close is shown in Fig. 6(d). Influenced by eyelash, the contour is not entirely the eyelids. However, it can be regarded as eyelids approximately to compare with the state of eyes-open.

Fig. 6. The eye area

For the shooting angle of the system is downwards, the result is not a kind of elliptic but an open up parabolic. Fit the profile curve with parabolic in least square method. Contrast of images eyes-open and eyes-close, it is easy to find that: The distance between upper and lower eyelids is smaller and the radius of curvature is smaller than eyes-open in middle position of upper eyelid, too. The change rate in height between upper and lower eyelids and in radius of curvature of fitted parabola

can be used to judge the eye's opening, which is the basis for the determination of fatigue.

4.2. Fatigue Recognition Based On PERCLOS

The paper selects *PERCLOS* method (P80) to judge driver fatigue. There are 25 frames per second. *A* unit time is 10 s (including 250 frames valid image), the *PERCLOS* value of f is:

$$f = \frac{N_c}{250} \times 100\% \tag{16}$$

where N_c is eye-close frame count during the time segment. *PERCLOS* threshold of Fatigue is set to 0.4. Whether driver situate in fatigue state can be recognized.

5. Experimental Results

The camera is *WATEC902H3* type Low illumination camera in experiment. It is used that Focal distance of 3.6, auto iris, self-design light source and *USB* image acquisition card. The infrared active illumination image acquisition system is installed in actual driving environment. 5 videos were recorded in the case of weak light at night. The result of detecting fatigue by the videos is shown in Fig. 7. Obviously, the system can locate the eyes of different drivers exactly when drivers watch the rearview mirror including other normal driving behavior. The result is not affected by the interference of the rear passengers. The recognition result is shown in Table 2.

Fig. 7. The real experiment of fatigue detection

Table 2. Test results of Fatigue

No.	Total Frames	Number Of Frames Positioning Eyes Correctly		Accuracy Rate Of Eye Location	Number Of Frames Judging Eye State Correctly	Accuracy Rate Of Eye State Recognition
1	5 325	4 851		91.10%	4 726	88.75%
2	8 664	7 818		90.24%	7 616	87.90%
3	9 316	8 513		91.38%	8 246	88.51%
4	12 648	11 642		92.05%	11 362	89.83%
5	15 313	14 059		91.81%	13 691	89.41%

The accuracy of eye location is more than 90%, and the accuracy of eyes state recognition is more than 87% in the 5 detection videos taken in night. The results show its good robustness when the angle is less than 30 degrees. Actually, the main reason of false identification is too large rotation head angle.

6. Conclusion

According to fatigue of night driving, the system uses infrared supplement light illumination imaging to improve the imaging quality and filter out the interference of ambient light without. Modified Fatigue detection algorithm improve the robustness of eye localization obviously and reduce the false rate of identification. After tested in real driving environment, the fatigue driving detection system has easy installation and low error rate. Generally, the excellent performance has important significance to develop the Fatigue driving test technique and reduce the rate of traffic accidents at night.

References

[1] A. H. Zuriaga, J. F. Berlanga, C. C. Moll: *Fatigue and driving. An empirical study.* Securitas Vialis *3.1* (2011), No. 1, 39–430.

[2] G. Zhang, K. K. W. Yau, X. Zhang: *Traffic accidents involving fatigue driving and their extent of casualties.* Accident Analysis & Prevention *87* (2016),34–42.

[3] J. Phipps, J. R. Redman, S. M. W. Rajaratnam: *Temporal profile of prolonged, night driving performance: breaks from driving temporarily reduce time fatigue but not sleepiness.* Journal of sleep research *20* (2011), No. 3, 405–415.

[4] M. J. Amin, N. A. Riza: *Active depth from defocus system using coherent illumination and a no moving parts camera.* Optics Communications *359* (2015), No. 5, 135–145.

[5] Z. Zhu, X. Qu, G. Jia: *Uniform illumination design by configuration of LED array and diffuse reflection surface for color vision application.* Display Technology, Journal of*7.2* (2011), No. 2, 84–89.

[6] Z. Zhang, J. Zhang: *A new real-time eye tracking based on nonlinear unscented Kalman filter for monitoring driver fatigue.*Journal of Control Theory and Applications *8.2* (2010), No. 2, 181–188.

[7] H. F. Wang, G. P. Wang, X. Y. Wang: *A kind of infrared expand depth of field vision sensor in low-visibility road condition for safety-driving.* Sensor Review *30* (2016), No. 1, 7–13.

Received November 16, 2017